Available online at www.sciencedirect.com

SCIENCE DIRECT®

Lithos 78 (2004) 25–42

LITHOS

www.elsevier.com/locate/lithos

# Melt extraction and accumulation from partially molten rocks

Paul D. Bons[a,*], Jochen Arnold[b], Marlina A. Elburg[c], Jaan Kalda[d], Alvar Soesoo[e], Boudewijn P. van Milligen[f]

[a]*Institut für Geowissenschaften, Eberhard Karls Universität Tübingen, Sigwartstrasse 10, D-72076 Tübingen, Germany*
[b]*Institut für Geowissenschaften, Johannes Gutenberg-Universität Mainz, D-55099 Mainz, Germany*
[c]*Max Planck Institute for Chemistry, Department of Geochemistry, Postfach 3060, D-55020 Mainz, Germany*
[d]*Institute of Cybernetics, Tallinn Technical University, Akadeemia tee 21, 12618 Tallinn, Estonia*
[e]*Institute of Geology, Tallinn Technical University, Estonia Ave 7, Tallinn 10143, Estonia*
[f]*Asociación Euratom-CIEMAT (Centro de Investigaciones Energéticas, Medioambientales y Tecnológicas), Avenida Complutense 22, 28040 Madrid, Spain*

Received 6 March 2003; accepted 23 April 2004
Available online 28 August 2004

**Abstract**

Current models for melt segregation and ascent are not adequate to accurately describe transport and accumulation in combination. We propose that transport is discontinuous and in batches, and that accumulation occurs by stepwise merging of batches. A simple numerical model of jostling spheres that merge when they touch was used to represent stepwise accumulation and transport of batches by propagation of hydrofractures. Results of the numerical model indicate that such a system may quickly develop into a self-organised critical (SOC) state. In this state, the distribution of melt batch volumes can be described by a power law, with an exponent $m$ that lies between 2/3 and 1. Once a self-organised critical state is established, the system is capable of discharging any additional melt without further change to itself. Deformation aids melt extraction efficiency, as it increases the mobility of hydrofractures, enhances accumulation and hence lowers the exponent $m$. Full connectivity of melt needs never to be reached in the system and melt transport and extraction can occur at very low melt fractions. The chemical evolution of melt from source to emplacement level will be governed by the discontinuous mixing and mingling of batches, each with different histories, and possibly different sources. If no subsequent homogenisation occurs in a magma chamber or the final emplacement structure, the process can be identified by chemical heterogeneity of plutons and volcanic rocks.


*Keywords:* Migmatite; Melt segregation; Magma ascent; Hydrofractures; Self-organised criticality

## 1. Introduction

Transfer of melt is the major mass transport and differentiation process in the Earth's crust and uppermost mantle, and answering the question of how this

* Corresponding author. Tel.: +49 7071 2976469; fax: +49 7071 5059.
*E-mail address:* paul.bons@uni-tuebingen.de (P.D. Bons).

0024-4937/$ - see front matter © 2004 Elsevier B.V. All rights reserved.
doi:10.1016/j.lithos.2004.04.041

process works is therefore of utmost importance (Brown, 1994; Sawyer, 1994; Bouchez et al., 1997; Petford et al., 2000). Three main models are currently advocated for the ascent of melt (Fig. 1)

(1) Diapirism envisages the mobilisation and slow ascent of buoyant magma or partially molten rock in large single volumes. Their ascent rate is controlled by ductile deformation of the surrounding host rock (e.g., Weinberg and Podladchikov, 1994; Paterson and Vernon, 1995).
(2) With dyking, magma ascends in discrete fractures or dykes. Magma flow rates are high relative to diapiric ascent and are controlled by viscous drag of the magma inside a dyke (e.g., Weertman, 1971; Spence and Turcotte, 1985; Lister and Kerr, 1991; Clemens and Mawer, 1992; Petford et al., 1993; Mériaux and Jaupart, 1998).
(3) Finally, magma may flow pervasively through pore space or fracture networks. The flow of magma is here controlled by the permeability of the system (e.g., Nicolas and Jackson, 1982; Collins and Sawyer, 1996; Weinberg and Searle, 1998; Brown and Solar, 1999; Vanderhaeghe, 1999; Weinberg, 1999; Leitch and Weinberg, 2002; Wark et al., 2003).

Although diapirism may be relevant to large-scale doming in the lower to middle crust (Teyssier and Whitney, 2002), consensus is developing that it is not a viable process to produce upper crustal plutons and magma chambers (e.g., Emerman and Marrett, 1990; Clemens and Mawer, 1992).

Two specific problems will be addressed in this paper:

(1) segregation and accumulation of melts and
(2) the process of mixing and mingling of different melt batches.

Because the melt transport mechanism directly constrains how these processes can take place, we focus on this, using a simple numerical model.

It should be noted here, that, for simplicity, we use the term "melt" throughout this paper. The term "melt" may then signify both a pure melt (without entrained crystals) or a "magma", which is melt that may contain entrained crystals.

### 1.1. Mixing and mingling

The vast majority of magmatic products (plutons, volcanic rocks) show evidence of an origin from multiple sources (McMillan et al., 1989; Leeman et al., 1990; Poli, 1992; Elliott et al., 1997; Gamble et al., 1999; Soesoo and Nicholls, 1999). The different sources may completely mix to form a range of hybrid phases or they may remain separate mingled phases; magmatic enclaves are the classical examples (Didier, 1987; Vernon et al., 1988; Poli and Tommasini, 1991; Elburg, 1996; Flinders and Clemens, 1996; Perugini and Poli, 2000; Perugini et al., 2003). Although it may be evident from the end product that mixing and mingling did take place, it is

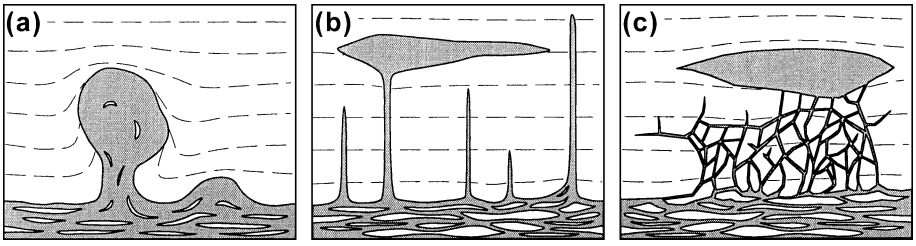


Fig. 1. Schematic sketches to illustrate the three dominant mechanisms for melt (grey) transport from a partially molten source below to a higher emplacement level. (a) Diapiric mobilisation of partially molten rock in large volumes. Wall rock is strongly deformed by rising diapers. Unmelted rock or restite may be entrained or partly left behind. (b) Melt ascent by dykes, that emanate from the partially molten source and may freeze, or drain into a magma chamber. (c) Melt ascent through a permeable medium; here, a network of fractures. Porous flow would also fall into this category.

less clear how and where these processes take place. Two basic end-member models can be envisaged:

(1) The phases interact in the source region, for example, by melting of different source rocks. Alternatively, high-temperature mafic (mantle) melts may intrude into crustal rocks, causing their melting, and may mix or mingle with them (Huppert and Sparks, 1988; Oliver and Barr, 1997). The mixed and mingled phases then ascend together.
(2) The other model envisages mixing and mingling after emplacement in a magma chamber. Different phases arrive at the magma chamber and the degree of mixing versus mingling depends on the dynamics of the chamber (convection, temperature, etc.; Sparks et al., 1977; Wiebe, 1987, 1988; Huppert, 1988; Wiebe and Snyder, 1993; Janousek et al., 2000; Wiebe et al., 2001; Perugini et al., 2003).

Hybrid models between these two end-members can be envisaged, where interaction takes place after melt generation, but before generation of the final batholith, during ascent in composite dykes (Collins et al., 2000) or channels (Spiegelman and Kelemen, 2003).

### 1.2. Accumulation

Within a partially melting crustal or upper mantle source, melt forms in very small volumes (approximately in cubic millimeters) on grain boundaries and microfractures (Rushmer, 1995; Sawyer, 2000; Klepeis et al., 2003; Guernina and Sawyer, 2003). The end product of melt transfer includes plutons and volcanic outpourings that can reach well over hundreds of cubic kilometers, which means that the transfer and segregation process leads to huge accumulation factors of over 20 orders of magnitude in volume. Despite the extensive research that has been dedicated to melt ascent, much less is known about the mechanism of accumulation. For example, it is still unclear how melt segregates from its source and accumulates to enter and feed a dyke (Sleep, 1988; Stevenson, 1989; Weinberg, 1999). A possible reason for this is that the focus of research has been on melt transport, not on accumulation. Transport models alone, such as Darcian theory for pervasive flow (e.g., McKenzie, 1984; Wickham, 1987; Weinberg, 1999) or conduit flow for dyking (e.g., Lister and Kerr, 1991; Mériaux and Jaupart, 1998) are primarily aimed at explaining transport. Segregation and accumulation may be involved, but as a secondary effect.

Gradients in melt hydraulic head or potential are needed to drive melt transport and accumulate melt. Such gradients may be caused by density differences, active deformation (e.g., folding) or magmatic intrusions into the source region (Sleep, 1988; Stevenson, 1989; Clemens and Mawer, 1992; Brown et al., 1995; Rubin, 1998). On the small scale, melt may reside in the pore space between grains, the geometry of which is often assumed to be controlled by the wetting angle (McKenzie, 1984; von Bargen and Waff, 1986). Flow in such a system is only possible when the pores are connected, which, again, depends on the wetting angle (von Bargen and Waff, 1986). At a low wetting angle, melt is connected by tubes along three-grain junctions. The melt fraction at which flow can effectively occur is currently regarded to be well below 10% (Rushmer, 1995; Vigneresse et al., 1996; Laporte et al., 1997; Renner et al., 2000; Faul, 2001).

Although the wetting angle may be very low (von Bargen and Waff, 1986), such porous flow is not effective when wall rock temperature is below the solidus temperature of the melt. It is becoming increasingly clear, both from field studies and experiments, that melt-induced embrittlement generally creates fractures in partially molten rocks on all scales from less than millimeter-scale microfractures to larger than meter-scale veins, sills and dykes (Weertman, 1971; Nicolas and Jackson, 1982; Sleep, 1988; Rubin, 1998; Rushmer, 1995; Connolly et al., 1997; Weinberg, 1999). Such melt-induced embrittlement is possible if the melt-pressure is, as usual, close to the lithostatic pressure and thus reduces the effective normal stresses to the point where extensional failure can occur (Secor, 1965).

Below, we briefly review current models for segregation and accumulation of melt to provide a background for our own numerical modelling.

#### 1.2.1. Porosity waves

The permeability ($\kappa$) of a partially molten rock is not constant, but is commonly regarded to be a

function of the melt fraction ($\phi$) by a power-law ($\kappa \propto \phi^P$), with an exponent $p$ that is typically assumed to be two or three (Dullien, 1979; von Bargen and Waff, 1986; Richardson et al., 1996; Wark and Watson, 1998). When $p \geq 2$, instabilities in the form of porosity waves can form (Schmeling, 2000; Rabinowicz et al., 2001): flow is enhanced where $\phi$ is high, leading to an influx of melt in these zones, which in turn leads to even more flow and melt influx. The coupling between flow and melt fraction leads to melt accumulation in the form of ascending high $\phi$ zones: porosity waves. These zones with fuzzy boundaries (gradients in melt fraction) should not be confused with dykes which result from brittle processes and have sharp boundaries between melt and solid wall rock. Porosity waves have been proposed for melt ascent in the mantle and for aqueous fluid transport within the crust (McKenzie, 1984; Connolly and Podladchikov, 1998, 2000; Rabinowicz et al., 2001), but are less likely of importance for melt transport through the crust, as dispersed melt in pores would freeze as soon as the matrix temperature is below the solidus temperature of the melt. Magma accumulation by porosity waves would inhibit the entrainment of any restitic material from the source of the magma, and would therefore not be a viable process for magmas with a low degree of melt–restite separation.

### 1.2.2. Fracture networks

A second model for the accumulation of melt, in particular, in the crust, is that of "rivulets feeding rivers": a connected network of fractures, whereby small fractures feed bigger ones (e.g., Weinberg, 1999). A first requirement of the model is that the fractures must organise in a hierarchical structure to focus flow and accumulate melt (Brown and Solar, 1998b). Secondly, enough fractures (and hence melt) must be present to establish connectivity to enable flow (Vigneresse et al., 1996). The connected fractures model is essentially a "barrier model"; flow must be established through a barrier that separates a source area from a destination area on the other side. Flow only occurs once connectivity is achieved across the barrier; that is, when the percolation threshold (Stauffer, 1985) is exceeded. The amount of flow (flux) is then determined by the permeability of the system and the driving gradient in hydraulic head across the barrier.

It is questionable whether the barrier concept is entirely applicable to describe segregation, escape and accumulation of melt from a source, where melt is progressively produced *within* the transport medium. When melt forms within its transport medium, it starts to flow as soon as there is local percolation and a gradient in hydraulic head (Vigneresse and Burg, 2000). Melt will flow to the most favourable site, leading to draining of fractures or porosity at some sites and local accumulation of melt at other sites. Melt segregation and accumulation may thus occur well below the percolation threshold for a particular melt geometry (pores, fractures), which fits in well with increasing evidence for low melt fractions in source rocks of some magmas (e.g., McKenzie and O'Nions, 1991) and almost complete draining of melt from some source rocks (Guernina and Sawyer, 2003). It is therefore doubtful whether a fully percolating fracture network is ever achieved, and if so, whether it can be maintained for any significant time. The absence of full percolation would invalidate flow models that rely on this percolation assumption (e.g., Weinberg, 1999; Leitch and Weinberg, 2002).

### 1.2.3. Stepwise accumulation and ascent

Melt- or fluid-filled hydrofractures become unstable when they exceed a certain length (Weertman, 1971; Secor and Pollard, 1975; Takada, 1990; Dahm, 2000; Bons et al., 2001; Menand and Tait, 2002). The instability arises from gradients in effective normal stress that may act on a hydrofracture along its length (Weertman, 1971). This can result from the increase in lithostatic pressure with depth which differs from the increase in pressure inside a steep or vertical hydrofracture if the density of the melt is different from that of the wall rock. This limits the vertical length of a melt-filled hydrofracture to several tens to hundreds of meters (Secor and Pollard, 1975). Stress gradients that arise from deformation in heterogeneous media or thermal instabilities may be up to the order of 1 MPa/m, which could make hydrofractures unstable that are less than 1 m in length (Secor and Pollard, 1975). Once instability is reached, a hydrofracture may start

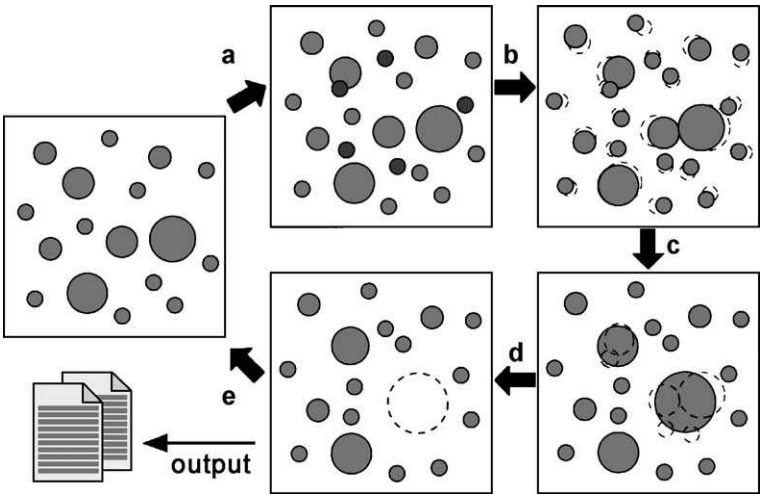


Fig. 2. Cycle of events that is carried out for every time step in the numerical model. Melt batches are represented by grey spheres. Note that the actual model is three-dimensional. (a) Addition of new small melt batches, typically 100 at a time. (b) Movement of all batches by a small distance, given by $E$, in a random direction. (c) Merging of overlapping batches into single batches. One merger can lead to new overlaps, and the process is repeated until no batches overlap. (d) Removal of batches that exceed the critical threshold volume, $V_{extrude}$. (e) Recording statistics of the system.

to propagate at one end, and simultaneously close at the other end if insufficient melt flows into the hydrofracture at the same time. The hydrofracture is therefore *mobile* and moves together with its content (Weertman, 1971; Secor and Pollard, 1975; Maaløe, 1987; Takada, 1990; Bons, 2001; Bons et al., 2001; Bons and van Milligen, 2001).

Transport in mobile hydrofractures would be stepwise and discontinuous in time and space; one hydrofracture would remain stagnant until the critical stress gradient is exceeded and the ensuing mechanical instability causes propagation of the hydrofracture. Propagation of a hydrofracture can then lead to interaction and mergers with other hydrofractures (Ito and Martel, 2002). The effect is a highly dynamic system with occasional and local bursts of hydrofracture propagation (transport) that cause avalanches of instabilities and mergers of hydrofractures (accumulation; Bons et al., 2001; Bons and van Milligen, 2001). Such a system cannot be described in terms of classical Darcian theory for continuos flow through fracture networks (van Milligen and Bons, 2002; Bons and Arnold, 2003).

Below, we will investigate the effect and dynamics of stepwise transport and accumulation with a simple numerical model.

## 2. Numerical modelling

### 2.1. Description of the model

The aim of the numerical model is to investigate the effect of stepwise segregation and accumulation of melt batches during progressive melting of a source region, assuming that melt resides and moves solely in mobile hydrofractures or veins.

The concept is that melt quickly moves from the grain boundaries where it forms into discrete batches in the form of veins. The small veins grow by addition of melt and new veins continually form with progressive melting. Growing neighbouring veins at some point touch and merge to form a single vein. Interaction of the veins is enhanced by the mobility of the veins under the influence of normal stress gradients along the veins (Secor and Pollard, 1975). Tectonic stress gradients can be up to about two orders of magnitude greater than those caused by the buoyancy of melt. Deformation is therefore an important factor for the mobility, and hence, the frequency of interaction and merging of the veins. This leads to a cascading or stepwise accumulation of small veins into bigger veins (Bons and van Milligen, 2001). With increasing size, buoyancy forces become increasingly important for the mobility of the veins.

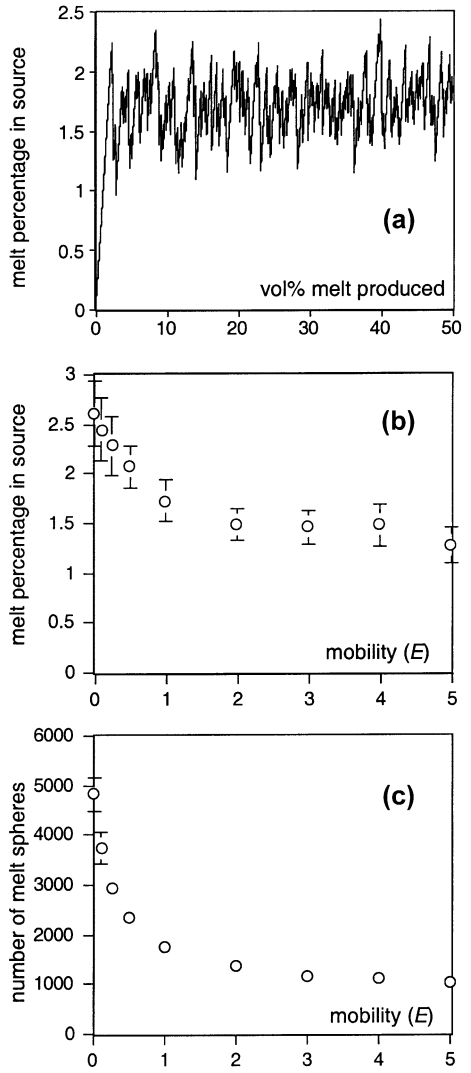


Fig. 3. (a) Graph of the melt percentage as a function of total percentage of melt that is produced, where 0.01% melt is added every step and the mobility $E$=1. A dynamic equilibrium melt fraction sets in within a few percent of melt addition. (b) Average melt percentage as a function of $E$. (c) Number of melt spheres in the unit cell as a function of $E$. Averaging is over the period from $t$=2000 to $t$=5000. Error bars equal one $\sigma$.

Large steeply oriented veins therefore preferentially move upwards. Veins eventually leave the system as dykes, when they are large enough to be able to ascend through cooler crust above without freezing.

In the numerical model, melt-filled veins are modelled as discrete spheres. It will become clear later that the admittedly unrealistic spherical shape does not significantly change the outcome. Progressive melting is simulated in discrete time steps, typically 5000 steps. Each step, the model goes through the following cycle (Fig. 2):

(1) Creating melt batches. 0.01% "melt" is added to a unit–cell cube of dimensions 100×100×100. The melt is added in the form of randomly placed small spheres, typically 100 spheres with a starting volume ($V_{min}$) of 1.

(2) Moving melt batches. The mobility of hydrofractures due to tectonic stress gradients is simulated by moving all spheres each step over a distance that is randomly chosen between $\pm E$ in the $x$-, $y$- and $z$-direction. $E$ (ranging from 0 to 5) is a measure of the mobility of the spheres. If a sphere moves outside of the cube, it reappears inside the cube at the opposite side (fully wrapping boundaries). One could expect large hydrofractures to be more mobile than smaller ones because the critical stress gradient at which a hydrofracture becomes unstable and may start to propagate is a function of the length of a hydrofracture (Weertman, 1971; Secor and Pollard, 1975). However, large tectonic stress gradients can only occur over small ranges, making smaller hydrofractures more prone to be mobilised than larger ones. The net effect of these two competing factors is unknown, and we therefore made $E$ independent of sphere size. Tectonic stress gradients may lead to propagation in any direction, while buoyancy forces would lead to upward propagation. A preferred upward propagation is not included, to reduce the number of parameters. This implies that the model applies to the region and scale where tectonic forces dominate over buoyancy-driven melt transport.

(3) Merging of melt batches. Of two connecting melt veins, one is usually likely to be more favourably oriented relative to tectonic stresses and gravity forces. Melt would move from the unfavourably oriented vein to the other. In our model, this is simulated by merging all pairs of overlapping or touching spheres. This is done after each round of creating and moving spheres and continued until no spheres overlap or touch each other. The new position of a new sphere is

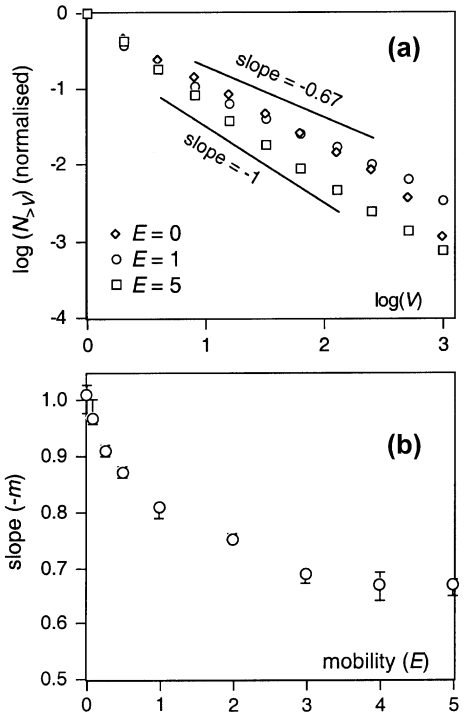


Fig. 4. (a) Logarithmic graph of the number of spheres larger than a certain volume versus that volume for three different mobilities ($E$). Total number of spheres is normalised to 1. (b) Graph of the distribution coefficient ($m$) as a function of $E$. Numbers of spheres were counted and added up every 250 time steps from $t$=2000 to $t$=5000. Circles indicate the slope for sphere sizes ranging from $V$=4 to $V$=256. The error bars bracket the slopes for the size ranges $V$=4 to 128 and $V$=8 to 256. Slopes were calculated with a nonweighted least-squares power-law fit to the data.

taken as the volume-weighted average of the centres of the two merged spheres. Checking whether spheres overlap is the most time-consuming step in the program, and limits the maximum number of spheres that can be modelled within a reasonable time to about 10,000.

(4) Extraction of melt batches. Finally, any sphere that exceeds a set threshold in volume ($V_{extrude}$) is removed from the cube, simulating the escape of a melt batch from the source region. The typical threshold volume of $V_{extrude}$=2000 represents the accumulation of at least 2000 initial spheres. It should be noted that the system is not volume conservative: when melt is lost from the system when a sphere is extracted, the size of the system is not reduced accordingly, but is kept at $100\times100\times100$ units. This simplification permits the study of a possible steady-state development without any long-term trends. Notice that, except for this fourth step, the model is similar to that for droplet growth of Family and Meakin (1988, 1989).

(5) Recording data. Statistics of the system and the extruded batches are recorded every time step.

### 2.2. Modelling results: melt distribution in the source

Within less than 200 time steps (<2% melting), the model system establishes a dynamic equilibrium where the extraction rate of melt spheres on average equals the addition rate (Fig. 3a). The average volume fraction of spheres, $\phi$, is about 2.6% when spheres are not moved ($E$=0) and decreases with increasing melt mobility to about 1.5% at $E\geq2$ (Fig. 3b). The melt fraction fluctuates strongly with variations of >0.5%. The average number of spheres in the system is a function of $E$. It is about 5000 for $E$=0 and reduces to about 1000 for $E$>2 (Fig. 3c).

Once dynamic equilibrium is reached, the sphere size distribution remains constant. The relationship between the number of spheres larger than a certain volume ($N_{>V}$) and that volume ($V$) can be approximated by a power-law (Fig. 4a):

$$N_{>V} = KV^{-m} \quad (1)$$

where $K$ is a constant (the number of spheres larger than unit volume) and $m$ the distribution exponent. The exponent $m$ is a function of the mobility $E$, decreasing from 1 for $E$=0 to 2/3 for $E\geq4$ (Fig. 4b). The distribution exponent $m$ describes the relationship between number of large and small spheres. A small value ($m$<1) signifies relatively few small spheres, compared to the number when $m$ is close to 1. A small value of $m$ also means that most of the volume contained by the spheres resides in the larger spheres. The fact that $m$ decreases with increasing $E$ means that accumulation becomes more efficient with increasing mobility, as would be expected.

Assuming that the power-law function of Eq. (1) describes the size distribution of the spheres, we can now use this equation to investigate how the settings of smallest and largest allowed sphere sizes influence the total volume contained by all spheres and the total

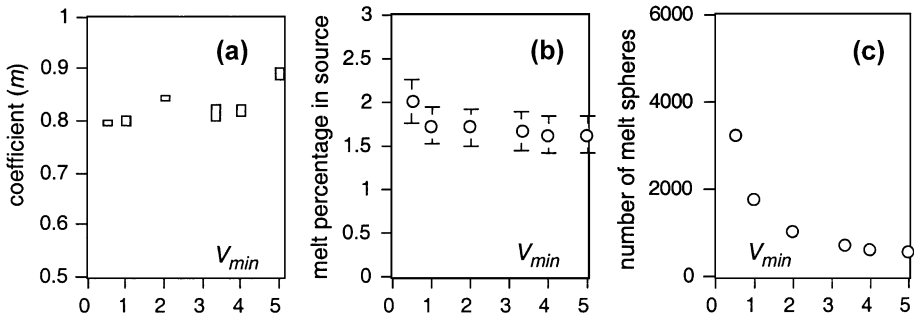


Fig. 5. (a) Sphere size distribution coefficient ($m$), (b) average melt percentage and (c) average number of spheres, as a function of initial sphere size ($V_{min}$) for $E$=1. The number of added spheres per time step is adjusted to maintain 0.01% melt addition per step. Bars in panel a represent the range in values for $m$ calculated from the size ranges $V$=4 to 128 and $V$=8 to 256. Error bars in panel b represent one $\sigma$.

number of spheres, and compare these with the results of the numerical experiments. The frequency ($f_V$) of spheres of a certain volume can be derived from Eq. (1):

$$f_V = \frac{-\partial N_V}{\partial V} = mKV^{-m-1} \tag{2}$$

The total volume $A_{V_a,V_b}$ of spheres in a size range $V_a$ to $V_b$ is (for $m \neq 1$):

$$A_{V_a,V_b} = \int_{V_a}^{V_b} V f_V \mathrm{d}V = \int_{V_a}^{V_b} mKV^{-m}\mathrm{d}V$$
$$= \left(\frac{m}{1-m}\right)K\left(V_b^{1-m} - V_a^{1-m}\right) \tag{3}$$

If $m$<1 and $V_b \gg V_a$, Eq. (3) can be approximated by:

$$A_{V_a,V_b} \approx \left(\frac{m}{1-m}\right)KV_b^{1-m} \tag{4}$$

Eq. (4) shows that the total volume of all spheres in the cube is mostly related to the size of largest sphere that is allowed ($V_b$=$V_{extrude}$) and not by the size of the smallest spheres ($V_{min}$) which has dropped out of the equation. This can be seen in Fig. 5, where the size of the initially created spheres is varied, while all other parameters are kept the same as for Figs. 3 and 4 and $E$=1. Fig. 5a and b show that $m$ and $\phi$ are not much influenced by the setting of $V_{min}$. The total number of spheres ($N_{total}$) is strongly affected by the setting of $V_{min}$ (Fig. 5c), but as $m \leq 1$, the many small spheres for small $V_{min}$ contain only a small fraction of the total melt volume.

Eq. (4) should hold for the case that $V_b \gg V_a$, which equates to $V_{extrude} \gg V_{min}$ in the numerical experiments. This was tested by running experiments with varying $V_{extrude}$. Fig. 6a shows that the condition is met, and $m$ settles at about 0.8 (for $E$=1), when $V_{extrude} \geq 1000$. Fig. 6a also shows that if $V_{extrude}$ is set too small, relative to $V_{min}$, the size range is too small for a power-law size distribution to develop. The setting of $V_{extrude}$ has little effect on $N_{total}$, but does

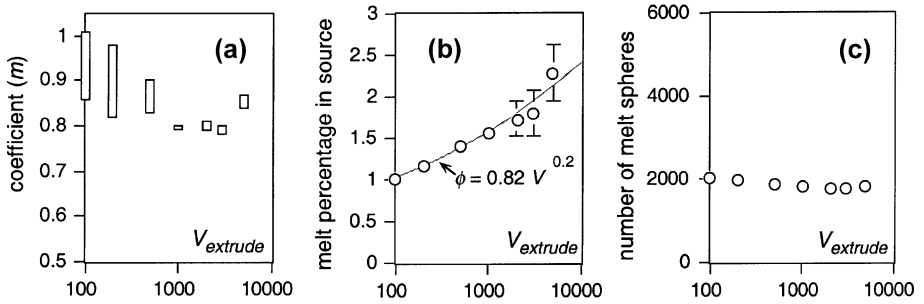


Fig. 6. (a) Sphere size distribution coefficient ($m$), (b) average melt percentage and (c) average number of spheres, as a function of maximum sphere size ($V_{extrude}$) for $E$=1. Bars in panel a represent the range in values for $m$ calculated from the size ranges $V$=4 to 128 and $V$=8 to 256. Error bars in panel b represent one $\sigma$.

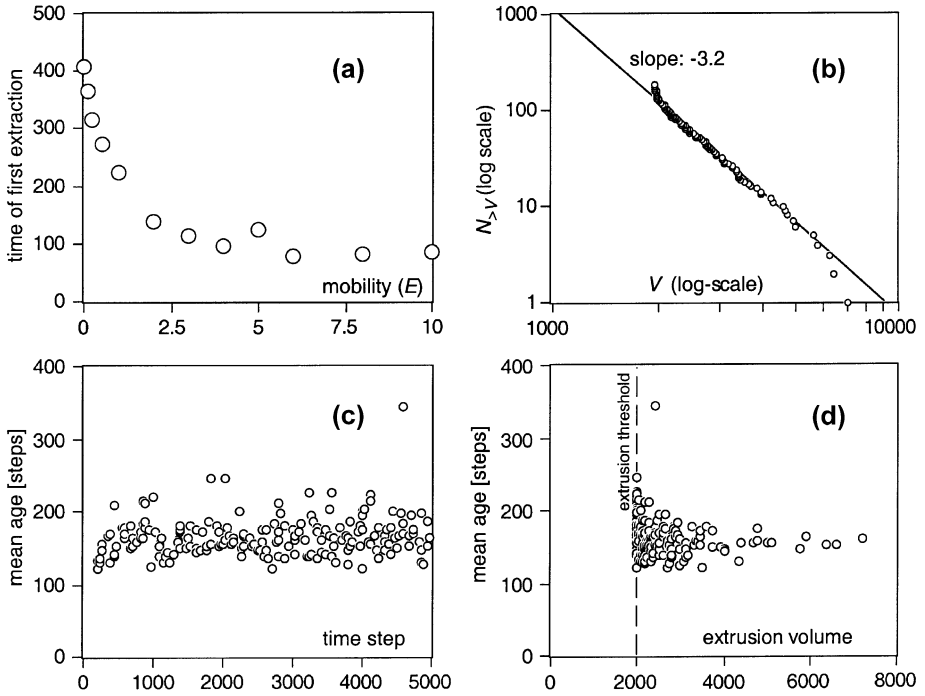


Fig. 7. (a) Onset of melt extraction as a function of mobility $E$. (b) Number of extruded spheres larger than $V$ as a function of $V$ in a logarithmic graph, showing a power-law distribution with a size distribution coefficient of 3.2. (c) Mean age of extrusions as a function of extrusion time. (d) Mean age of extrusions as a function of volume of extruded melt batch. Data for $E$=1, $V_{min}$=1 and $V_{extrude}$=2000.

have an effect on the average melt fraction (Fig. 6). As can be expected from Eq. (4), $\phi = A_{V\min, V\text{extrude}}$ has a power-law relation with $V_{extrude}$, with an exponent of $1-m$ (=0.2 for $E$=1) as long as $V_{extrude} \gg V_{min}$.

In summary, the size distribution of spheres in the numerical experiments is well described by the power-law Eq. (1) and its derivatives, as long as $V_{min}$ is small enough compared to $V_{extrude}$, a condition that is met with the settings $V_{min}$=1 and $V_{extrude}$=2000.

### 2.3. Modelling results: melt extraction from the source

Spheres that are larger than $V_{extrude}$ are removed from the cube. This simulates the ascent and escape of the largest melt veins or dykes from the source region. It is clear that the time needed to accumulate the largest spheres is related to the mobility ($E$). High mobility causes efficient accumulation and hence a low distribution coefficient $m$ and an early onset of extraction (Fig. 7a). Because two or more spheres close to $V_{extrude}$ in size can merge, the size of extracted spheres can range from $V_{extrude}$ to several times that volume, although most are close to $V_{extrude}$ in volume. It is interesting to note that the size distribution of extruded spheres also follows a similar power-law distribution as the spheres inside the cube, but with a much larger distribution coefficient of around 3.2 (Fig. 7b).

In a geological context, the extruded spheres would represent batches of melt that are emplaced at higher levels, either as individual dykes or as batches entering a higher level pluton or magma chamber. Each of these batches may have a different chemistry, due to differences in source rock or differences in time of melting and accumulation history (Stephens, 1992; Hobden et al., 1999; Sobolev et al., 2000). In the numerical model, the time of this creation of an initial sphere is recorded as an attribute of that sphere. This attribute is a simple proxy of the chemistry of the melt and is assumed not to be further modified by interaction with the wall rock. With each merger of spheres, the creation times of the two merging spheres are volume-weighted averaged, simulating the geochemical effect of mixing of different melt batches.

The average age of the melt in an extracted pocket can now be defined as the average time from creation of melt to its extraction. The average age is about 150 steps for $E$=1 (Fig. 7c), which is the time needed for 1.5% melting. The smallest extracted batches have the highest variability in age (Fig. 7d). The mobility factor $E$ has a distinct effect on the character of the population of extruded spheres. With increasing $E$, the average size of the extracted batches decreases and the average age decreases, but the variability of ages increases. In geological terms, this implies that a high deformation rate within the source would favour many, but small batches to leave the source and a high variability in melt chemistry, reflecting the relatively short residence time within the source.

## 3. Discussion

### 3.1. The distribution exponent

The numerical experiments produced power-law distributions with a distribution exponent ranging from $m \approx 1$ for $E$=0 (spheres not moved) down to $m \approx 2/3$ when spheres are very mobile ($E \geq 4$). Eq. (3) shows that $m$=1 is a special case. When $m$>1, the integral must be taken from the smallest batch size, as most mass resides in the smallest batches. When $m$<1, most mass resides in the largest batches: mass is accumulated. $m$=1 can be regarded as representing the boundary between dispersion and accumulation.

$m$=2/3 represents a second special case, where 50% of all mass resides in the single largest batch within the system. This represents very strong concentration, with effectively all mass residing in a few batches and a negligible amount of mass in all smaller batches. The experiments produced $m$<1 when spheres were moved ($E$>0). In that case, agglomeration is controlled by coalescence of batches that encountered each other during their movement.

Our numerical model, employing spheres as batch shapes, as well as analogue experiments with gas-filled lenticular hydrofractures (Bons and van Milligen, 2001) indicate that a power-law size distribution will emerge from stepwise accumulation or aggregation of batches. This power-law equation (Eq. (1)) describes the distribution of volumes of batches, irrespective of their shape, as shape is not a parameter in the equation. The range of values that the exponent $m$ can take ($2/3<m<1$ for accumulation) is therefore also independent of the shape of batches, as long as a power-law describes the volume distribution of the batches.

Processes in which particles move according to some specified rules, collide and form larger particles (agglomerates of smaller particles) are described by the Smoluchowski equation (von Smoluchowski, 1917). This equation has been used to model various processes, such as polymerisation, coagulation, aggregation (Vicsek and Family, 1984) and droplet nucleation (Family and Meakin, 1989; Cueille and Sire, 1998). In this approach, the scaling exponent of the particle size distribution depends on the scaling of a collision kernel, which, in turn, depends on details of particle motion and interaction. Our numerical results of $m$=1 for $E$=0, decreasing to $m$=2/3 for $E \gg 1$, are in agreement with analytical scaling estimates (Debierre, 1989; Cueille and Sire, 1998).

### 3.2. Self-organised criticality

The system utilised in this paper bears some typical characteristics of self-organised criticality (SOC) (Bak et al., 1988). In the SOC state, a system adjusts itself to accommodate transport, whereas in a Darcian or conduit-flow system, the transport (flux) adjusts itself to the system. For melt transport, this means that the rock matrix is modified to allow transport to happen at the rate determined by the melting rate. A typical feature of a SOC system is that there is a strongly dynamic balance between input and output and that any small perturbation can (but need not) lead to a large chain reaction or avalanche. The classical example for a SOC system is the sand pile, built by sprinkling sand grains at the apex (Bak et al., 1988; Hwa and Kardar, 1992). The slope of the pile remains constant on average, but is highly dynamic. Each added grain may come to rest on the slope, but may also cause the whole slope to collapse in a large slide. Phenomena in such systems, such as the size of the sand avalanches, are typically self-similar; that is, they show power-law distributions, such as those observed in our melt accumulation model.

The computer model that is presented here also shows a dynamic balance between input of melt and

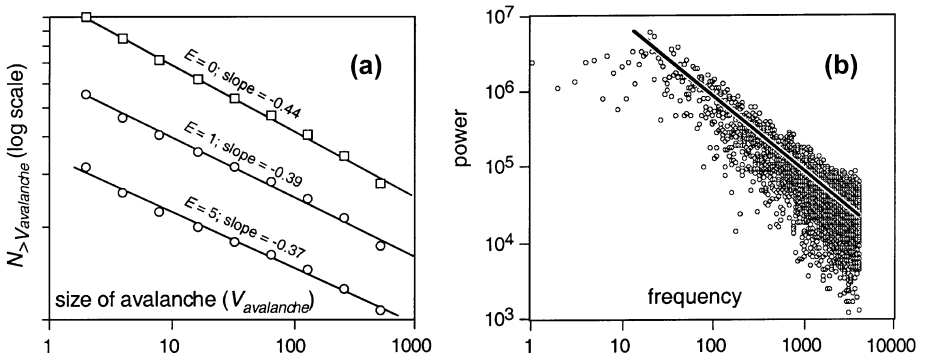


Fig. 8. (a) Number of "avalanches" (see text for definition) larger than a certain volume ($V_{avalanche}$) as a function of $V_{avalanche}$ for three different mobilities. Numbers are normalised to different values so that the data do not overlap. In a log–log graph, this only shifts data up or down, but does not affect their slope and therefore no numbers are given along the $y$-axis. (b) $1/f$—behaviour in the power spectrum of total volume of melt in model over 8192 steps, starting from $t$=1808, for the case $E$=0. $V_{min}$=1 and $V_{extrude}$=2000 in both graphs.

extraction and power-law size distributions of spheres inside the cube as well as of extracted spheres. An analogue to the avalanches of the sand pile model can also be found in the melting model. New small melt batches may quietly remain where they formed, or they may cause a merger with other melt batches, possibly leading to a chain reaction that results in the formation of a large melt batch that can leave the source region. Each such avalanche was recorded in the model. The magnitude of an avalanche was taken as the final volume of the sphere that resulted from one continuous series of mergers. The smallest and most common avalanche size is 2, formed by the merger of two initial spheres. As can be expected in a SOC system, these avalanches also show a power-law size distribution, with a distribution coefficient $m \approx 0.4$ (Fig. 8a).

Another characteristic of a SOC state is that fluctuations are not random. When a signal (e.g., amount of melt in source) fluctuates randomly, its power spectrum is flat. This means that all frequencies of fluctuations have the same magnitude or "power". SOC systems typically show so-called $1/f$ power spectra, meaning that the power of fluctuations is inversely proportional to their frequency ($f$) (Bak et al., 1987). Fig. 3a shows that the melt percentage within the numerical model fluctuates strongly. The power spectrum of the melt percentage in one experiment ($E$=0) was calculated with a fast-Fourier-transform over 8192 time steps (starting at $t$=1808, to avoid effects of initial settling of the system). Fig. 6b shows that the power spectrum of the melt percentage is not flat (random noise), but can be approximately described as $1/f$.

The power-law distribution of spheres was not enforced from outside in the model. Instead, it always develops by itself: the system is *self-organised*. The system also quickly reaches a *critical* state where any added spheres may lead to a chain reaction of avalanches, and where all added spheres are discharged on average.

### 3.3. Implications for melt transport and accumulation

The computer model, in all its simplicity, may give some insight in the way in which melt is accumulated and extracted from partially molten sources. First of all, if such systems are self-organised critical (SOC), melt transport and accumulation is not a steady continuous process, but occurs in many small and occasionally large bursts (Bak et al., 1988; Bons and van Milligen, 2001). This is difficult to describe with classical equations for flow through permeable media, such as employed by, e.g., McKenzie (1984), Sleep (1988), Schmeling (2000) and Connolly and Podladchikov (1998). Instead, stochastic models need to be devised that describe the punctuated transport and the accumulation and extraction of melt.

Once the system has reached its SOC state (in the model, within a few percent of melting), melting rate and extraction rate balance on average. The average rate of melt extraction is then only dependent on the melting rate and not on the mobility and hence deformation rate. However, the deformation rate is

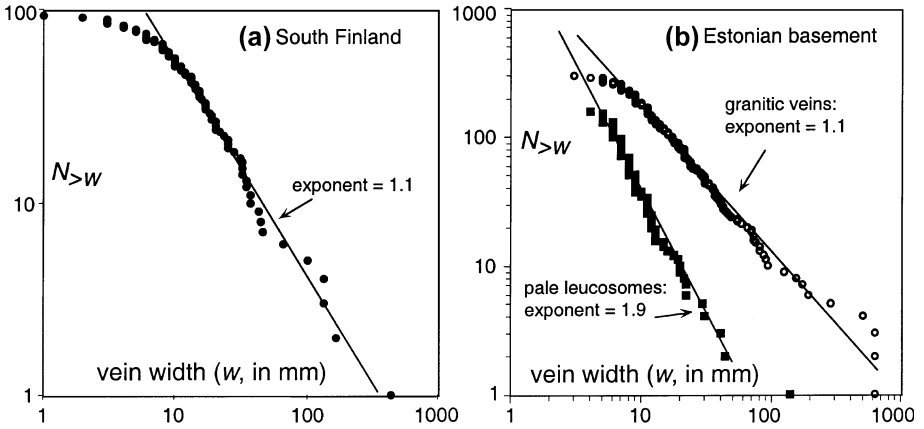


Fig. 9. Cumulative frequency plot of vein widths in migmatites, taken along a linear section. Number of veins wider than a certain width are plotted against that width. (a) 92 veins, measured over a 5-m section perpendicular to stromatic foliation at the "Masku Riviera", north of Turku in southern Finland. The veins make up 31% of the whole section. A power-law best fit through all veins wider than 10 mm gives a distribution exponent of 1.1. (b) Drill core Nr 156 from Vägeva in eastern Estonia. 450 veins were measured in a 40-m section at a high angle (~70°) to the stromatic foliation. The veins make up 24% of the whole section. Pale fine-grained leucosomes are plotted separately from coarser-grained pink–orange granitic veins. A power-law best fit through all veins wider than 5 to 10 mm give exponents of 1.9 (■) and 1.1 (○), respectively.

important because it determines the type of SOC state (e.g., distribution coefficient $m$), how quickly it is reached and the characteristics of the extruded batches. High deformation rates favour an early onset of extraction (Fig. 7a) because accumulation is efficient and large volumes are quickly formed. It also favours relatively many, but smaller extruded batches; and a high variability in residence time in the source.

The sharp cut-off value ($V_{extrude}$) for release of melt batches from the source is of course not realistic in the model. It makes an artificial distinction between the sphere size distribution within the model (the result of avalanches of mergers) and the size distribution of extracted spheres. In reality, the two can be envisaged to form a continuum, where the chances or viability of ascent would increase with volume. Larger and larger melt batches gradually move up through the system. As they leave their source area, they can only interact with other large batches, as small ones would freeze too quickly if the ambient temperature is below the solidus temperature of the melt. Gradually, going upwards, the process of buoyancy driven melt ascent in hydrofractures or dykes takes over from the melt segregation and accumulation that is described in the present model. Our model suggests that the mobility of the melt in the source would influence the size distribution of the largest escaping batches.

The self-similar distribution of melt batches implies that ascending dykes can be effectively no different from small melt veins or leucosomes, except for their size and dominant driving force for movement (buoyancy). They form the largest end-members of a continuum. Making a distinction between dyke ascent and melt segregation and accumulation then becomes just as artificial as our extraction at $V>V_{extrude}$. This has repercussions for dyke ascent models that postulate some sort of feeder point at which a certain influx or melt pressure is assumed (e.g., Lister and Kerr, 1991; Rubin, 1993; Mériaux and Jaupart, 1998; Menand and Tait, 2002). Such models may thus be inappropriate for dykes emanating from partial molten sources and may only be applicable to dykes sourced from magma chambers (Bons et al., 2001).

### 3.4. Application to melt distribution in natural systems

Power-law distributions are frequently found in fracture, vein and dyke populations (e.g., Kruhl, 1994; Tanner, 1999; Bonnet et al., 2001). We measured widths of magmatic veins in a stromatic migmatite at the "Masku Riviera" north of Turku, in the Paleoproterozoic Migmatite–Granite Belt of southern Finland (Ehlers et al., 1993; Lindroos et

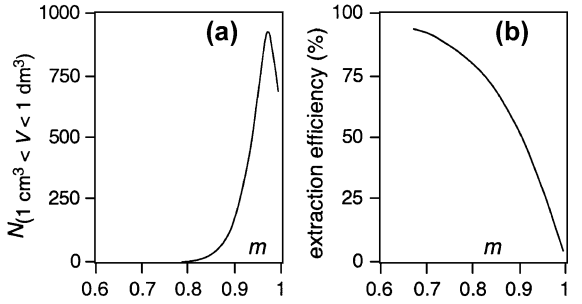


Fig. 10. (a) Number of melt batches between 1 $cm^3$ and 1 $dm^3$, per cubic metre as a function of $m$, for the case of 10% melting in 10-km rock column over 100×100 km area. (b) Melt extraction efficiency as a function of $m$, if in the previous case melt batches are extracted at a volume >1 $km^3$.

al., 1996), and in a drill core from the equivalent Estonian basement (Puura et al., 1997). In the Estonian drill core, a distinction could be made between pale fine-grained leucosomes and coarser, distinctly orange-pink granitic to pegmatitic veins. Each set of veins showed power-law distributions with exponents of 1.1 to 1.9 for veins wider than about 5 to 10 mm (Fig. 9). The deviation from the power-law trend for the smallest veins is at least, in part, the effect of undersampling of these smallest veins. Any natural size distribution must have upper and lower limits, and the breakdown of the power-law at the small sizes may therefore also indicate a lower limit of the power-law range, close to the grain size. Marchildon and Brown (2003) reported similar measurements of leucosome width distributions, but did not find clear power-law distributions. It should, however, be noted that their width range was mostly in the range of 1 to 10 mm, and may have suffered the same cut-off effect at the small end of the range.

The width distribution exponent along a linear sampling section cannot be simply equated with the volume distribution exponent $m$. The purpose of the examples is merely to show that power-law distributions of melt batches are indeed found in nature, consistent with our proposed model.

We will now quantitatively apply the outcomes of the numerical model to natural partial melt systems. We use the previous inference that all accumulated melt batches, whether remaining in the source or extracted, form a continuous range, defined by the distribution coefficient $m$.

To obtain a value of the total volume of melt that is produced ($A_{tot}$), we must define an area where melting takes place and the amount of melting per unit area. For crustal melting, the area is constrained by a characteristic length scale within which the melting can be regarded as forming one system. Such a length scale would be in the order of ten to a hundred kilometers, and we arbitrarily choose 100 km here, to obtain an area of 100×100 km=$10^4$ $km^2$. A total melting of 1 $km^3$ per $km^2$ crustal column seems a reasonable value (Zen, 1992), which then gives $A_{tot}=10^4$ $km^3$.

To determine the number of melt batches of any size in a system, we need to determine $K$ (as defined in Eq. (1)). $K$ can be determined by using the fact that, per definition, there is only one batch as large as the largest batch, which we call $V_{max}$. This can be inserted into Eq. (1), giving:

$$N_{>V_{max}} = KV_{max}^{-m} = 1 \Leftrightarrow V_{max} = K^{1/m} \tag{5}$$

Combining Eqs. (4) and (5) then gives the value of $K$ as a function of the total melt volume ($A_{tot}$) and the distribution coefficient $m$:

$$K = \left(\frac{(1-m)A_{tot}}{m}\right)^{m} \tag{6}$$

Knowing $K$, one can use Eq. (1) to calculate the number of melt veins of a certain size range, for instance, those between 1 $cm^3$ and 1 $dm^3$ in volume. The above example of 1 $km^3$ melting per $km^2$ crustal column, assuming melting occurs over a 10-km depth range, gives ~0.03 ($m$=0.67) to ~900 ($m$=0.97) of such veins per $m^3$ (Fig. 10a). Finally, we can determine a melt extraction efficiency if we define an extraction volume threshold above which melt batches are extracted from the source. If, in the above example, the extraction threshold volume is set at 1 $km^3$, about 94% is extracted if $m$=0.67, and the extraction efficiency reduces to zero at $m$=1 (Fig. 10b).

We see that the SOC system can describe the full range from zero accumulation ($m$=1) to almost complete accumulation ($m$=2/3). Chemical analyses indicate that many granulite rocks experienced melt loss (Guernina and Sawyer, 2003), but physical traces of this melt or its pathways are rare. Our results indicate that it is possible to efficiently drain

melt from a source, when $m \approx 2/3$, in which case little evidence would remain in the form of leucosomes.

### 3.5. Geochemical implications

Like the cellular automaton of Vigneresse and Burg (2000), our model indicates that the interaction between melt and source may not be simple, and might not be described meaningfully by average values. Some batches of melt have a long residence time, while others may quickly become entrained in large accumulation avalanches and have little time to interact with the restite or other melt. Melt chemistry may be variable from one extracted batch to another. Although melt batches that were extracted late contain, on average, melt that was formed late, occasionally, they may contain significant proportions of early-formed melt. In any case, there is always some "delay" between melt formation and extraction, and the melt that formed last has less chance of being extracted. Estimates of total melt percentage from extracted melts would then underestimate the total melt production in the source by this delay amount.

The proposed model has several implications for the geochemistry of melts formed by this process. Because melt escapes from the source before a percolation threshold or "critical melt percentage" (Arzi, 1978; van der Molen and Paterson, 1979; Vigneresse et al., 1996) has been reached, melt extraction starts at an earlier stage than in conventional models of granite petrogenesis especially if melt extraction is enhanced by deformation (Ayres et al., 1997; Oliver and Barr, 1997; Brown and Solar, 1998a). This may leave the melt only a limited amount of time to equilibrate with its restite or melanosome and could lead to disequilibrium partitioning of trace elements (Cambray et al., 1995; Harris et al., 1995; Bea, 1996) and even isotopes (Tommasini and Davies, 1997). Granites formed according to this model would fail to "image their sources" (Chappell, 1984) and attempts to model the composition of the source by equilibrium partitioning between melts and restite would be doomed to fail (Sawyer, 1991). In the case that each melt batch managed to reach equilibrium with its source, we would expect to see distinct geochemical differences between different batches of melt, reflecting the amount of previous melt depletion. The geochemistry of the successive melt batches would then approach that expected from incremental batch melting.

Both processes (disequilibrium melting and incremental batch melting) will lead to geochemical distinctions between different melt batches. If these melt batches coalesce and solidify at a higher crustal level, the resulting batholith may show internal heterogeneity, provided cooling is quick enough to inhibit rehomogenisation by, for instance, thermal and chemical convection. Observed heterogeneity in batholiths is often interpreted as the result of inhomogeneous distribution of crystal phases [either phenocrystic (Weaver et al., 1992) or restitic (Chappell, 1996)] or the result from in situ differentiation (Michael, 1984), but several studies have shown that the internal (geochemical) structure of some plutonic complexes can best be explained by the coalescence of distinct melt batches (Stephens, 1992; Wareham et al., 1997; Pressley and Brown, 1999; Slater et al., 2001; Waight et al., 2001; Perugini et al., 2003; Spiegelman and Kelemen, 2003).

Our model applies equally well to granitic magmatism as to basaltic magmatism. Advances in microanalytical technology has allowed the recognition of distinct populations of melt inclusions within single olivine crystals from ocean island basalts (Sobolev et al., 2000), arc basalts (Schiano et al., 2000) and mid-ocean ridge basalts (Kamenetsky et al., 1998). The existence of such small-scale heterogeneities indicates that melt generation in these tectonic environments is also dominated by small melt batches that only later coalesce to form the voluminous basaltic outpourings observed in oceanic islands or island arcs. Studies of short-lived isotopes in arc lavas yield similar results (Thomas et al., 2002). Ascent of mafic magmas in small melt batches through the crust is a very efficient way to heat and melt the crust. Small batches have a relatively large surface area and can therefore efficiently interact with the crust, causing fractional crystallisation of the mafic melt and concomitant assimilation (AFC, DePaolo, 1981).

The heterogeneity in many plutons and volcanics, in the form of mixing and mingling structures, should also be reconsidered in the light of our proposed model. We emphasize again that the power-law distributions imply a continuum from small magmatic veins to large dykes and final emplacement structures, which are actually no

more than large melt batches that became frozen. There is no sharp distinction between source, ascent structures, in-between magma chambers and final emplacement structures. Mixing and mingling occurs anywhere within this hierarchical accumulation and ascent system, as differentiated melt batches of the same source and melt batches from other sources merge and interact. There is no need to infer a single magma chamber somewhere in the path between source and emplacement for mixing and mingling to take place.

## 4. Conclusions

Most models for melt segregation and ascent do not explain transport and accumulation of melt *in combination*. Our model, based on the assumption that melt batches reside in hydrofractures, explains both transports by hydrofracture propagation and stepwise accumulation by hydrofracture merging. The model predicts that the system quickly develops into a self-organised critical state, where the melt distribution is organised in a self-similar way to allow discharge of any additional melt. The melt distribution can be described by a power law with an exponent $m$ (Eq. (1)), which ranges between 2/3 and 1, irrespective of actual shape of melt batches.

The stepwise melt transport and accumulation we propose does not separate the process from source to emplacement in distinct phases, but instead links the smallest melt batch (leucosome) to the largest emplacement structure (batholith) in one single holistic system.

## Acknowledgements

MAE acknowledges financial support from a European Union Marie Curie Fellowship. AS and JK acknowledge financial support from the Estonian Science Foundation (grant Nr. 5301 and 5036, respectively). JA acknowledges financial support from the DFG *Graduiertenkolleg* in Mainz: “Composition and evolution of crust and mantle”. Data from Finland were collected with a grant from the Dutch Dr. Schürmann Foundation for Precambrian research. We thank the two reviewers for the many improvements they suggested.

## References

Arzi, A.A., 1978. Critical phenomena in the rheology of partially molten rocks. Tectonophysics 44, 173–184.

Ayres, M., Harris, N., Vance, D., 1997. Possible constraints on anatectic melt residence times from accessory mineral dissolution rates: an example from Himalayan leucogranites. Mineral. Mag. 61, 29–36.

Bak, P., Tang, C., Wiesenfeld, K., 1987. Self-organized criticality: an explanation of 1/f noise. Phys. Rev. Lett. 59, 381–384.

Bak, P., Tang, C., Wiesenfeld, K., 1988. Self-organized criticality. Phys. Rev., A 38, 364–374.

Bea, F., 1996. Controls on the trace element composition of crustal melts. Trans. R. Soc. Edinb. Earth Sci. 87, 33–41.

Bonnet, E., Bour, O., Odling, N.E., Davy, P., Main, I., Cowie, P., Berkowitz, B., 2001. Scaling of fracture systems in geological media. Rev. Geophys. 39, 347–383.

Bons, P.D., 2001. The formation of large quartz veins by rapid ascent of fluids in mobile hydrofractures. Tectonophysics 336, 1–17.

Bons, P.D., Arnold, J., 2003. Accumulation and self-organization in hydrofracture transport of fluids. J. Geochem. Explor. 78-79, 667–670.

Bons, P.D., van Milligen, B.P., 2001. A new experiment to model self-organized critical transport and accumulation of melt and hydrocarbons from their source rocks. Geology 29, 919–922.

Bons, P.D., Dougherty-Page, J., Elburg, M.A., 2001. Stepwise accumulation and ascent of magmas. J. Metamorph. Geol. 19, 627–633.

Bouchez, J.L., Hutton, D.H.W., Stephens, W.E. (Eds.), 1997. Granite: From Segregation of Melt to Emplacement Fabrics. Kluwer Academic Publishers, Dordrecht.

Brown, M., 1994. The generation, segregation, ascent and emplacement of granite magma: the migmatite-to-crustally-derived granite connection in thickened orogens. Earth-Sci. Rev. 36, 83–130.

Brown, M., Solar, G.S., 1998a. Granite ascent and emplacement during contractional deformation in convergent orogens. J. Struct. Geol. 20, 1365–1393.

Brown, M., Solar, G.S., 1998b. Shear-zone systems and melts: feedback relations and self-organization in orogenic belts. J. Struct. Geol. 20, 211–227.

Brown, M., Solar, G.S., 1999. The mechanism of ascent and emplacement of granite magma during transpression: a syntectonic granite paradigm. Tectonophysics 312, 1–33.

Brown, M., Averkin, Y.A., McLellan, E.L., Sawyer, E.W., 1995. Melt segregation in migmatites. J. Geophys. Res. 100, 15655–15679.

Cambray, F.W., Vogel, T.A., Mills, J.G., 1995. Origin of compositional heterogeneities in tuffs of the Timber Mountain Group: the relationship between magma batches and magma transfer and emplacement in an extensional environment. J. Geophys. Res. 100, 15793–15805.

Chappell, B.W., 1984. Source rocks of I- and S-type granites in the Lachlan Fold Belt, southeastern Australia. Phil. Trans. R. Soc. Lond. A 310, 693–707.

Chappell, B.W., 1996. Magma mixing and the production of compositional variation within granite suites: evidence from the granites of southeastern Australia. J. Petrol. 37, 449–470.
Clemens, J.D., Mawer, C.K., 1992. Granitic magma transport by fracture propagation. Tectonophysics 204, 339–360.
Collins, W.J., Sawyer, E.W., 1996. Pervasive granitoid magma transfer through the lower-middle crust during non-coaxial compressional deformation. J. Met. Geol. 14, 565–579.
Collins, W.J., Richards, S.R., Healy, B.E., Ellison, P.I., 2000. Origin of heterogeneous mafic enclaves by two-stage hybridisation in magma conduits (dykes) below and in granitic magma chambers. Trans. R. Soc. Edinb. Earth Sci. 91, 27–45.
Connolly, J.A.D., Podladchikov, Y.Y., 1998. Compaction-driven fluid flow in viscoelastic rock. Geodinamica Acta 11, 55–84.
Connolly, J.A.D., Podladchikov, Y.Y., 2000. Temperature-dependent viscoelastic compaction and compartmentalization in sedimentary basins. Tectonophysics 324, 137–168.
Connolly, J.A.D., Holness, M.B., Rubie, D.C., Rushmer, T., 1997. Reaction-induced microcracking: an experimental investigation of a mechanism for enhancing anatectic melt extraction. Geology 25, 591–594.
Cueille, S., Sire, C., 1998. Droplet nucleation and Smoluchowski's equation with growth and injection of particles. Phys. Rev. E 57, 881–900.
Dahm, T., 2000. On the shape and velocity of fluid-filled fractures in the earth. Geophys. J. Int. 142, 181–192.
Debierre, J., 1989. Chain-chain aggregation in three dimensions: a test of the Smoluchowski theory. Phys. Rev., A 40, 4804–4807.
DePaolo, D., 1981. Trace element and isotopic effects of combined wallrock assimilation and fractional crystallisation. Earth Planet. Sci. Lett. 53, 189–202.
Didier, J., 1987. Contribution of enclave studies to the understanding of origin and evolution of granitic magmas. Geol. Rundsch. 76, 41–50.
Dullien, F.A.L., 1979. Porous Media Fluid Transport and Pore Structure. Academic Press, New York.
Ehlers, C., Lindroos, A., Selonen, O., 1993. The late Svecofennian granite–migmatite zone of southern Finland—a belt of transpressive deformation and granite emplacement. Precambrian Res. 64, 295–309.
Elburg, M.A., 1996. Genetic significance of multiple enclave types in a peraluminous ignimbrite suite, Lachlan Fold Belt, Australia. J. Petrol. 37, 1385–1408.
Elliott, T., Plank, T., Zindler, A., White, W., Bourdon, B., 1997. Element transport from subducted slab to juvenile crust at the Mariana arc. J. Geophys. Res. 102, 14991–15019.
Emerman, S.H., Marrett, R., 1990. Why dikes? Geology 18, 231–233.
Family, F., Meakin, P., 1988. Scaling of the droplet-size distribution in vapor-deposited thin films. Phys. Rev. Lett. 61, 428–431.
Family, F., Meakin, P., 1989. Kinetics of droplet growth processes: simulations, theory, and experiments. Phys. Rev., A 40, 3836–3854.
Faul, U.H., 2001. Melt retention and segregation beneath mid-ocean ridges. Nature 410, 920–923.
Flinders, J., Clemens, J.D., 1996. Non-linear dynamics, chaos, complexity and enclaves in granitoid magmas. Trans. R. Soc. Edinb. Earth Sci. 87, 225–232.
Gamble, J.A., Wood, C.P., Price, R.C., Smith, I.E.M., Stewart, R.B., Waight, T., 1999. A fifty year perspective of magmatic evolution on Ruapehu Volcano, New Zealand: verification of open system behaviour in an arc volcano. Earth Planet. Sci. Lett. 170, 301–314.
Guernina, S., Sawyer, E.W., 2003. Large-scale melt-depletion in granulite terranes: an example from the Archean Ashuanipi Subprovince of Quebeq. J. Metamorph. Geol. 21, 181–201.
Harris, N., Ayres, M., Massey, J., 1995. Geochemistry of granitic melts produced during the incongruent melting of muscovite: implications for the extraction of Himalayan leucogranite magmas. J. Geophys. Res. 100, 15767–15777.
Hobden, B.J., Houghton, B.F., Davidson, J.P., Weaver, S.D., 1999. Small and short-lived magma batches at composite volcanoes: time windows at Tongariro volcano, New Zealand. J. Geol. Soc. (London) 156, 865–868.
Huppert, H., 1988. Melting the roof of a chamber containing a hot, turbulently convecting fluid. J. Fluid Mech. 188, 107–131.
Huppert, H., Sparks, R.S.J., 1988. The generation of granitic magmas by intrusion of basalt into continental crust. J. Petrol. 29, 599–624.
Hwa, T., Kardar, M., 1992. Avalanches, hydrodynamics, and discharge events in models of sandpiles. Phys. Rev., A 45, 7002–7023.
Ito, G., Martel, S.J., 2002. Focusing of magma in the upper mantle through dike interaction. J. Geophys. Res. 107, 2223.
Janousek, V., Bowes, D.R., Braithwaite, C.J.R., Rogers, G., 2000. Microstructural and mineralogical evidence for limited involvement of magma mixing in the petrogenesis of a Hercynian high-K calc–alkaline intrusion: the Kozárovice granodiorite, Central Bohemian Pluton, Czech Republic. Trans. R. Soc. Edinb. Earth Sci. 91, 15–26.
Kamenetsky, V.S., Eggins, S.M., Crawford, A.J., Green, D.H., Gasparon, M., Falloon, T.J., 1998. Calcic melt inclusions in primitive olivine at 43N MAR: evidence for melt–rock reaction/melting involving clinopyroxene-rich lithologies during MORB generation. Earth Planet. Sci. Lett. 160, 115–132.
Klepeis, K.A., Clarke, G.L., Rushmer, T., 2003. Magma transport and coupling between deformation and magmatism in the continental lithosphere. GSA Today, 4–11. (January).
Kruhl, J.H., 1994. The formation of extensional veins: an application of the Cantor-dust model. In: Kruhl, J.H. (Ed.), Fractals and Dynamic Systems in Geoscience. Springer Verlag, Berlin, pp. 95–104.
Laporte, D., Rapaille, C., Provost, A., 1997. Wetting angles, equilibrium melt geometry, and the permeability threshold of partially molten crustal protoliths. In: Bouchez, J.L., et al., (Eds.), Granite: From Segregation of Melt to Emplacement Fabrics. Kluwer Academic Publishers, Dordrecht, pp. 31–54.
Leeman, W.P., Smith, D.R., Hildreth, W., Palacz, Z., Rogers, N., 1990. Compositional diversity of late Cenozoic basalts in a transect across the southern Washington Cascades: implications for subduction zone magmatism. J. Geophys. Res. 95, 19561–19582.
Leitch, A.M., Weinberg, R.F., 2002. Modelling granite migration by mesoscale pervasive flow. Earth Planet. Sci. Lett. 200, 131–146.

Lindroos, A., Romer, R.L., Ehlers, C., Alviola, R., 1996. Late-orogenic Svecofennian deformation in SW Finland constrained by pegmatite emplacement ages. Terra Nova 8, 567–574.
Lister, J.R., Kerr, R.C., 1991. Fluid-mechanical models of crack propagation and their application to magma transport in dykes. J. Geophys. Res. 96, 10049–10077.
Maaløe, S., 1987. The generation and shape of feeder dykes from mantle sources. Contrib. Mineral. Petrol. 96, 47–55.
Marchildon, N., Brown, M., 2003. Spatial distribution of melt-bearing structures in anatectic rocks from Southern Brittany, France: implications for melt transfer at grain- to orogen-scale. Tectonophysics 364, 215–235.
McKenzie, D., 1984. The generation and compaction of partially molten rocks. J. Petrol. 25, 713–765.
McKenzie, D., O'Nions, K., 1991. Partial melt distributions from inversion of rare earth element concentrations. J. Petrol. 32, 1021–1091.
McMillan, N.J., Harmon, R.S., Moorbath, S., Lopez-Escobar, L., Strong, D.F., 1989. Crustal sources involved in continental arc magmatism: a case study of volcan Mocho-Choshuenco, southern Chile. Geology 17, 1152–1156.
Menand, T., Tait, S.R., 2002. The propagation of buoyant fluid-filled fissure from a source under constant pressure: an experimental approach. J. Geophys. Res. 107, 2306.
Mériaux, C., Jaupart, C., 1998. Dike propagation through an elastic plate. J. Geophys. Res. 103, 18295–18314.
Michael, P.J., 1984. Chemical differentiation of the Cordillera Paine granite (southern Chile) by in situ fractional crystallization. Contrib. Mineral. Petrol. 87, 179–195.
Nicolas, A., Jackson, M., 1982. High temperature dikes in peridotites: origin by hydraulic fracturing. J. Petrol. 23, 568–582.
Oliver, N.H.S., Barr, T.D., 1997. The geometry and evolution of magma pathways through migmatites of the Halls Creek Orogen, Western Australia. Mineral. Mag. 61, 3–14.
Paterson, S.R., Vernon, R.H., 1995. Bursting the bubble of ballooning plutons: a return to nested diapirs emplaced by multiple processes. Geol. Soc. Amer. Bull. 107, 1356–1380.
Perugini, D., Poli, G., 2000. Chaotic dynamics and fractals in magmatic interaction processes: a different approach to the interpretation of mafic microgranular enclaves. Earth Planet. Sci. Lett. 175, 93–103.
Perugini, D., Poli, G., Christofides, G., Eleftheriadis, G., 2003. Magma mixing in the Sithonia Plutonic Complex, Greece: evidence from mafic microgranular enclaves. Mineral. Petrol. 78, 173–200.
Petford, N., Kerr, R.C., Lister, J.R., 1993. Dike transport of granitoid magmas. Geology 21, 845–848.
Petford, N., Cruden, A.R., McCaffrey, K.J.W., Vigneresse, J.-L., 2000. Granite formation, transport and emplacement in the Earth's crust. Nature 408, 669–673.
Poli, G., 1992. Geochemistry of Tuscan Archipelago Granitoids, central Italy: the role of hybridization processes in their genesis. J. Geol. 100, 41–56.
Poli, G., Tommasini, S., 1991. Origin and significance of micro-granular inclusions in calc–alkaline granitoids: a proposed working model. J. Petrol. 32, 657–666.
Pressley, R.A., Brown, M., 1999. The Phillips pluton, Maine, USA: evidence of heterogeneous crustal sources and implications for granite ascent and emplacement in convergent orogens. Lithos 46, 335–366.
Puura, V., Klein, V., Koppelmaa, H., Niin, M., 1997. Precambrian basement. In: Raukas, A., Teedumäe, A. (Eds.), Geology and Mineral Resources of Estonia. Estonian Academy Publishers, Tallinn, pp. 27–34.
Rabinowicz, M., Genthon, P., Ceuleneer, G., Hillairet, M., 2001. Compaction in a mantle mush with high concentrations and the generation of magma chambers. Earth Planet. Sci. Lett. 188, 313–328.
Renner, J., Evans, B., Hirth, G., 2000. On the rheologically critical melt fraction. Earth Planet. Sci. Lett. 181, 585–594.
Richardson, C.N., Lister, J.R., McKenzie, D., 1996. Melt conduits in a viscous porous matrix. J. Geophys. Res. 101, 20423–20432.
Rubin, A.M., 1993. Dikes vs. diapirs in viscoelastic rock. Earth Planet. Sci. Lett. 117, 653–670.
Rubin, A.M., 1998. Dike ascent in partially molten rock. J. Geophys. Res. 103, 20901–20919.
Rushmer, T., 1995. An experimental deformation study of partially molten amphibolite: application to low-melt fraction segregation. J. Geophys. Res. 100, 15681–15695.
Sawyer, E., 1991. Disequilibrium melting and the rate of melt–residuum separation during migmatization of mafic rocks from the Grenville Front, Quebeq. J. Petrol. 32, 701–738.
Sawyer, E.W., 1994. Melt segregation in the continental crust. Geology 22, 1019–1022.
Sawyer, E.W., 2000. Grain-scale and outcrop-scale distribution and movement of melt in a crystallising granite. Trans. R. Soc. Edinb. Earth Sci. 91, 73–85.
Schiano, P., Eiler, J.M., Hutcheon, I.D., Stolper, E.M., 2000. Primitive CaO-rich, silica-undersaturated melts in island arcs: evidence for the involvement of clinopyroxene-rich lithologies in the petrogenesis of arc magmas. Geochem. Geophys. Geosyst. 1 (1999GC000032).
Schmeling, H., 2000. Partial melting and melt segregation in a convecting mantle. In: Bagdassarov, N., Laporte, D., Thompson, A.B. (Eds.), Physics and Chemistry of Partially Molten Rocks. Kluwer Academic Publ., Dordrecht, pp. 141–178.
Secor, D.T., 1965. Role of fluid pressure in jointing. Am. J. Sci. 263, 633–646.
Secor, D.T., Pollard, D.D., 1975. On the stability of open hydraulic fractures in the Earth's crust. Geophys. Res. Lett. 2, 510–513.
Slater, L., McKenzie, D., Grönvold, K., Shimizu, N., 2001. Melt generation and movement beneath Theistareykir, NE Iceland. J. Petrol. 42, 321–354.
Sleep, N.H., 1988. Tapping of melt by veins and dikes. J. Geophys. Res. 93, 10255–10272.
Sobolev, A.V., Hofmann, A.W., Nikogosian, I.K., 2000. Recycled oceanic crust observed in 'ghost plagioclase' within the source of Mauna Loa Lavas. Nature 404, 986–990.
Soesoo, A., Nicholls, I.A., 1999. Mafic rocks spatially associated with Devonian felsic intrusions of the Lachlan Fold Belt: a possible mantle contribution to crustal evolution processes. Aust. J. Earth Sci. 46, 725–734.

Sparks, R.S.J., Sigurdsson, H., Wilson, L., 1977. Magma mixing: a mechanism for triggering acid explosive eruptions. Nature 267, 315–318.
Spence, D.A., Turcotte, D.L., 1985. Magma-driven propagation of cracks. J. Geophys. Res. 90, 575–580.
Spiegelman, M., Kelemen, P.B., 2003. Extreme chemical variability as a consequence of channelized melt transport. Geochem. Geophys. Geosyst. 4, 1055 (doi:10.1029/2002GC000336).
Stauffer, D., 1985. Introduction to Percolation Theory. Taylor and Francis, London.
Stephens, W.E., 1992. Spatial, compositional and rheological constraints on the origin of zoning in the Criffell pluton, Scotland. Trans. R. Soc. Edinb. Earth Sci. 83, 191–199.
Stevenson, D.J., 1989. Spontaneous small-scale melt segregation in partial melts undergoing deformation. Geophys. Res. Lett. 16, 1067–1070.
Takada, A., 1990. Experimental study on propagation of liquid-filled crack in gelatin: shape and velocity in hydrostatic stress condition. J. Geophys. Res. 95, 8471–8481.
Tanner, D.C., 1999. The scale-invariant nature of migmatite from the Oberpfalz, NE Bavaria and its significance for melt transport. Tectonophysics 302, 297–305.
Teyssier, C., Whitney, D.L., 2002. Gneiss domes and orogeny. Geology 30, 1139–1142.
Thomas, R.B., Hrschmann, M.M., Cheng, H., Reagan, M.K., Edwards, R.L., 2002. ($^{231}$Pa/$^{235}$U)–($^{230}$Th/$^{238}$U) of young mafic volcanic rocks from Nicaragua and Costa Rica and the influence of flux melting on U-series systematics of arc lavas. Geochim. Cosmochim. Acta 66, 4287–4309.
Tommasini, S., Davies, G.R., 1997. Isotope disequilibrium melting during anatexis: a case study of contact melting, Sierra Nevada, California. Earth Planet. Sci. Lett. 148, 273–285.
Vanderhaeghe, O., 1999. Pervasive melt migration from migmatites to leucogranite in the Sushwap metamorphic core complex, Canada: control of regional deformation. Tectonophysics 312, 35–55.
van der Molen, I., Paterson, M.S., 1979. Experimental deformation of partially melted granite. Contrib. Mineral. Petrol. 70, 299–318.
van Milligen, B.P., Bons, P.D., 2002. Comment on "Hillslope evolution by nonlinear creep and landsliding. An experimental study, by Roering, J.J., Kirchner, J.W., Sklar, L.S. and Dietrich, W.E.". Geology 30, 481–482.
Vernon, R.H., Etheridge, M.E., Wall, V.J., 1988. Shape and microstructure of microgranitoid enclaves: indicators of magma mingling and flow. Lithos 22, 1–11.
Vicsek, T., Family, F., 1984. Dynamic scaling for aggregation of clusters. Phys. Rev. Lett. 52, 1669–1672.
Vigneresse, J.-L., Burg, J.P., 2000. Continuous vs. discontinuous melt segregation in migmatites: insights from a cellular automaton model. Terra Nova 12, 188–192.
Vigneresse, J.-L., Barbey, P., Cuney, M., 1996. Rheological transitions during partial melting and crystallization with application to felsic magma segregation and transfer. J. Petrol. 37, 1579–1600.
von Bargen, N., Waff, H.S., 1986. Permeabilities, interfacial areas and curvatures of partially molten systems: results of numerical computations of equilibrium microstructures. J. Geophys. Res. 91, 9261–9276.
von Smoluchowski, M., 1917. Versuch einer mathematischen Theorie der Koagulations-Kinetik von kolloid Lösungen. Z. Phys. Chem. 92, 129–135.
Waight, T.E., Wiebe, R.A., Krogstad, E.J., Walher, R.J., 2001. Isotopic responses to basaltic injections into silicic magma chambers; a whole-rock and microsampling study of macro-rhythmic units in the Pleasant Bay layered gabbro-diorite complex, Maine, USA. Contrib. Mineral. Petrol. 142, 323–335.
Wareham, C.D., Vaughan, A.P.M., Miller, I.L., 1997. The Wiley Glacier complex, Antarctic Peninsula: pluton growth by pulsing of granitoid magmas. Chem. Geol. 143, 65–80.
Wark, D.A., Watson, E.B., 1998. Grain-scale permeabilities of texturally equilibrated, monomineralic rocks. Earth Planet. Sci. Lett. 164, 591–605.
Wark, D.A., Williams, C.A., Watson, E.B., Price, J.D., 2003. Reassessment of pore shapes in microstructurally equilibrated rocks, with implications for permeability of the upper mantle. J. Geophys. Res. 108 (2001JB001575).
Weaver, S.D., Adams, C.J., Pankhurst, R.J., Gibson, I.L., 1992. Granites of Edward VII Peninsula, Marie Byrd Land: anorogenic magmatism related to Antarctic–New Zealand rifting. Trans. R. Soc. Edinb. Earth Sci. 83, 281–290.
Weertman, J., 1971. Theory of water-filled crevasses in glaciers applied to vertical magma transport beneath ocean ridges. J. Geophys. Res. 76, 1171–1183.
Weinberg, R.F., 1999. Mesoscale pervasive felsic magma migration: alternatives to dyking. Lithos 46, 393–410.
Weinberg, R.F., Podladchikov, Y.Y., 1994. Diapiric ascent of magmas through power law crust and mantle. J. Geophys. Res. 99, 9543–9559.
Weinberg, R.F., Searle, M.P., 1998. The Pangong Injection Complex, Indian Karakoram: a case of pervasive granite flow through hot viscous crust. J. Geol. Soc. (London) 155, 883–891.
Wickham, S.M., 1987. The segregation and emplacement of granitic magmas. J. Geol. Soc. (London) 144, 281–297.
Wiebe, R.A., 1987. Rupture and inflation of a basic magma chamber by silicic liquid. Nature 326, 69–71.
Wiebe, R.A., 1988. Structural and magmatic evolution of a magma chamber: the Newark Island layered intrusion, Nain, Labrador. J. Petrol. 29, 383–411.
Wiebe, R.A., Snyder, D., 1993. Slow, dense replenishments of a basic magma chamber: the Newark Island layered intrusion, Nain, Labrador. Contrib. Mineral. Petrol. 113, 59–72.
Wiebe, R.A., Frey, H., Hawkins, D.P., 2001. Basaltic pillow mounds in the Vinalhaven intrusion, Main. J. Volcanol. Geotherm. Res. 107, 171–184.
Zen, E., 1992. Using granite to image the thermal state of the source terrain. Trans. R. Soc. Edinb. Earth Sci. 83, 107–114.